Microbiological Research 220 (2019) 61–71

Contents lists available at ScienceDirect

Microbiological Research

journal homepage: www.elsevier.com/locate/micres

Sestrin-like protein from *Dictyostelium discoideum* is involved in autophagy under starvation stress

S. Rafia[1], S. Saran*,[1]

School of Life Sciences, Jawaharlal Nehru University, New Delhi, 110067, India

ARTICLE INFO

Keywords:
Dictyostelium
Sestrin
Autophagy
ROS
AMPK
Stress

ABSTRACT

Sestrins are highly conserved; stress inducible proteins that help maintain metabolic homeostasis and protect cells under stress conditions. They are up-regulated during stress and influence AMPK and mTOR pathways. Our objective was to find the role of Sestrin protein from *Dictyostelium discoideum (Dd)*, a lower eukaryote where starvation stress initiates multicellular development. The single *DdSesn-like* gene was expressed and its endogenous functions were characterized. Both, the knockout and constitutively expressing strains were made and their involvement in starvation-induced autophagy was analyzed. Autophagic fluxes and ROS levels were also monitored. Additionally, overexpression of *DdSesn* decreased cell growth and showed a longer lag phase. Upon starvation both *DdSesn* and ROS levels increased. $Sesn^{OE}$ showed reduced ROS levels while $sesn^{-}$ showed increased ROS levels when compared to the wild type. Therefore, we suggest that increased *sesn* expression may be beneficial in reducing ROS levels during starvation. Deletion of *sesn* showed reduced autophagic flux and increased p4EBP1 levels. We show that DdSesn promotes autophagy in *D. discoideum* upon starvation.

1. Introduction

In nature, organisms face various types of stress due to the constantly changing environment that may threaten their survival. Therefore, to provide protection against life-threatening challenges and to restore normal physiological and metabolic homeostasis, they adapt various kinds of stress responses to meet the overall fitness. In recent times, researchers discovered the evolutionarily conserved, stress-inducible Sestrin proteins (Sesns) named after Sestri Levante, a small town on the Ligurian coast of Italy, whose expression is induced during various environmental stress such as DNA damage, oxidative stress and hypoxia (Budanov et al., 2010). Mammals express three Sestrins (1–3) (Peeters et al., 2003), while *Drosophila melanogaster* and *Caenorhabditis elegans* have single orthologs (Lee et al., 2010). The invertebrates have only one *sestrin* (*sesn*) gene while the yeast does not have any. Sesn1 is p53-induced (Velasco-Miguel et al., 1999), Sesn2 is genotoxic or oxidative stress-induced (Budanov et al., 2002) and Sesn3 is activated in response to cell stimulation by serum or growth factors (Chen et al., 2010). Sesns exhibit antioxidant response(s) due to its oxido-reductase activity (Budanov et al., 2004) thus, protecting cells from oxidative stress. Sesn2 could up-regulate autophagic catabolism by inhibiting mTOR (Lee et al., 2012; Bae et al., 2013), however it is still not understood how it activates autophagy. Sesns are important regulators of metabolic homeostasis; accordingly, inactivation of *sesn* gene in invertebrates results in diverse metabolic pathologies, including oxidative damage, fat accumulation, mitochondrial dysfunction and muscle degeneration, that resemble accelerated tissue aging (Lee et al., 2010). Also, deletion of *sesn* genes in mice led to metabolic diseases (Lee et al., 2013).

Presently, we aim to explore the function and regulation of Sesn in *Dictyostelium discoideum,* a protist whose development is initiated under starvation stress and thus requires mechanisms to mobilize resources that could help maintain cellular homeostasis, which largely depends on macroautophagy (now referred to as autophagy). They show autophagy similar to mammals rather than yeast (King, 2012). TORC1 regulates translation by phosphorylating its downstream targets, namely the protein kinase p70S6K1 and the 4E-BP1 proteins (Showkat et al., 2014). Another important function of TORC1 is to inhibit autophagy, a process of sequestration and lysosomal degradation of intracellular organelles (including mitochondria), cytoplasmic content (Klionsky et al., 2016) and plays an important role in the control of cell viability by providing the necessary nutrients during adverse situations like starvation. Inhibition of TOR activity can be monitored by phosphorylation of p70S6K1, 4E-binding protein (4E-BP1) and S6 proteins (Wullschleger et al., 2006).

Dictyostelium amoebae grow and divide mitotically till food is

* Corresponding author.
E-mail addresses: rafia267@gmail.com (S. Rafia), ssaran@mail.jnu.ac.in, shweta_saran@hotmail.com (S. Saran).
[1] Both the authors approved the manuscript.

https://doi.org/10.1016/j.micres.2018.12.006
Received 23 February 2018; Received in revised form 12 December 2018; Accepted 28 December 2018
Available online 28 December 2018

available but upon starvation and in response to the chemoattractant, cAMP, these amoebae collect at common collecting points to form aggregates, which undergo various morphogenetic movements to finally culminate into fruiting bodies (Schaap, 2011) consisting of two terminally differentiated cell types: stalk (dead-vacuolated) and spore (viable) cells. The precursors of these cells are named prestalk and prespore, respectively and are observed at earlier stages of development and show transdifferentiation. *D. discoideum* follows developmental cell death where approximately 10–15% of the total population forms stalk cells involving autophagic cell death (Whittingham and Raper, 1960). Autophagy is a major cellular pathway for the degradation of organelles and proteins in eukaryotic organisms and shows evolutionary conservation between yeast and human. It is induced in response to both extracellular and intracellular stress conditions. During induction of autophagy, a double-membrane vesicle called autophagosomes begins to form in the cytosol, which engulfs components to be degraded. The outer membranes of the autophagosomes then fuse to the vacuolar/lysosomal membrane and release the inner vesicle, called autophagic body, into the vacuole/lysosomal. Lower eukaryotes use this for survival while higher eukaryotes use this for a variety of physiological and pathological processes (reviewed in Klionsky et al., 2016). It is thus important to find how the Sesn protein is involved in autophagy during development of this organism.

Here, we describe the function(s) of the Sesn-like protein from *D. discoideum,* which is expressed in the prestalk/stalk cells and is involved in autophagy. Our results show an increase in reactive oxygen species (ROS) as well as *sesn* mRNA levels upon starvation. We also show that overexpression of DdSesn reduced TOR levels besides increasing the phosphorylated adenosine monophosphate-activated protein kinase (pAMPK) levels.

2. Materials and methods

2.1. Dictyostelium growth and development

Dictyostelium discoideum, Ax2 (wild type) cells and the mutants were grown and developed as described earlier (Gosain et al., 2012). Logarithmic phase cultures (~3–5 × 10^6 cells/ml) were identically diluted into fresh liquid media at a density of 5–10 × 10^5 cells/ml and cell growth was monitored over several days.

Cell size was monitored using flow cytometry (Becton Dickinson, FACS Calibur) and the data was acquired using Cell-Quest software.

Development was carried as mentioned in Gosain et al. (2012). Briefly, exponentially growing cells were harvested, washed in 1xKK_2 buffer and spotted at a density of 5 × 10^7 cells/ml on non-nutrient agar plates. The plates were synchronized for development by incubating at 4 °C for 6 h. Subsequently, they were incubated at 22 °C for development to proceed.

2.2. Multiple sequence alignment and phylogenetic analysis

The genomic DNA, cDNA and protein sequences of DdSesn were obtained from the online resource (http://www.dictybase.org). Simple Modular Architecture Research Tool (SMART, http://SMART.embl-heidelberg.de) was employed to deduce domain architectures of the proteins. Orthologs of DdSesn were searched at NCBI (http://blast.ncbi.nlm.nih.gov/Blast.cgi), Uniprot (www.uniport.org) and dictyBase (http://www.dictybase.org). Protein sequences with significant E-values were selected by ruling out the hypothetical or predicted and unnamed proteins along with incomplete and redundant sequences from the first 1000 displayed sequences. Prior to the construction of the phylogenetic tree (http://www.phylogeny.fr), multiple sequence alignment was performed using protein sequences using MUSCLE software (Edgar, 2004). Following this, with the help of G block software, gaps were removed and the Maximum Likelihood (ML) tree was constructed using PhyML program (Guindon and Gascuel, 2003; Guindon et al., 2005). Sequences showing insignificant branch support from the final constructed tree were removed manually and the tree was re-rooted using TreeDyn (Dereeper et al., 2008) in Newick format and visualized under MEGA6.0. program (Tamura et al., 2013).

Functional domains in DdSesn were predicted by multiple sequence alignments carried out with the full-length DdSesn protein sequence and the individual known domains of HsSesn2 (Sesn-A, Sesn-B, Sesn-C domain regions).

The secondary structure of the *Dd*Sesn protein was predicted by using the Protein Homology/AnalogY Recognition Engine 2 (Phyre) server (http://www.sbg.bio.ac.uk.phyre2) which offers an automated protein structure prediction service. The query *Dd*Sesn protein sequence that was submitted to the server was first subjected to scanning against a large sequence database using PSI-BLAST by generating the profile which was further processed by the neural network secondary structure prediction program (PsiPred) and the protein disorder predictor (Disopred) to produce the predicted α-helices, β-strands and disordered regions that were shown graphically together with the colour-coded confidence bar. The phyre software built the secondary structure based on the best homologous leucine bound Sestrin2 (c5dj4d) sequence from *Homo sapiens,* which was used as template. The numbering for the helices is given manually with the help of other online servers namely PSIRED and YASPIN.

2.3. Spatiotemporal mRNA expression during development

2.3.1. RT-PCR

Cells from various stages of development were harvested and RNA was extracted using Trizol reagent (Sigma, USA) (Gosain et al., 2012). The cDNA was synthesized according to the manufacturer's instructions (Invitrogen). *rnlA* (*ig7)* was used as an internal control. Primer pairs used for the amplifications are listed in Table 1. The cycle numbers used for the amplifications were within the linear range (Fig. S1 A). The PCR (initial denaturation: 98 °C-3 min; cycle denaturation: 98 °C-45 s; annealing: 58 °C-45 s (52 °C-30 s for *ig7*); extension: 68 °C -1.2 min; final extension: 68 °C −10 min; forever: 4 °C) was performed for 24 cycles for both *ig7* and *sesn*.

2.3.2. In situ hybridization

The spatiotemporal mRNA expression in multicellular structures were studied by *in situ* hybridization using DIG-labelled RNA probe that was prepared by PCR amplification of exonic DNA from the full-length *sesn* gene (Gosain et al., 2012). The amplified product with XbaI and NotI sites was cloned in the pBSIISK + vector (gift from Prof Pauline Schaap, Dundee) having the promoters of T3 and T7 RNA polymerases. The construct pBSIISK + harboring the exonic DNA was digested with XbaI to yield template for antisense probe synthesis by T3 RNA polymerase, while digestion with NotI yield the template for sense probe synthesis by T7 RNA polymerase. Both sense and antisense probes were hydrolyzed into smaller sizes and used for *in vitro* transcription (Gosain et al., 2012). The photographs of various developmental structures were taken on Olympus (SMZ32) stereozoom microscope.

To obtain multicellular structures, Ax2 cells at a density of ~1 × 10^7cells/cm^2 were plated on non-nutrient agar plates and allowed to proceed in development. The multicellular structures thus developed were collected in 1x PBS buffer in small culture plates. The structures were further fixed at room temperature for 2.5 h in 100% methanol and 4% paraformaldehyde. The fixed structures were then permeabilized with proteinase K (20 μg/ml) in PBS, washed and pre-hybridized at 50 °C for 3 h. This was followed by hybridization with sense or antisense probe for 20 h at 50 °C. After removal of excess probe by successive washes, the samples were equilibrated with PBST containing 0.2% blocking solution and treated with anti-digoxigenin antibody (1:1000) coupled to alkaline phosphatase and kept at 4 °C overnight. After incubation, the structures were washed with phosphatase buffer and stained with 340 μg/ml NBT and 174 μg/ml BCIP in phosphatase buffer

Table 1
List of oligonucleotides used in this study.

Set	Oligo name	5'—— 3'	Genomic positions
1	RT-PCR-*sesn*	FP- AGTATGGGAATGACAAGTAAAGGC	7-30
		RP- ACAACAACTACAACAACAACTACCAAC	1,486-1,513
2	RT-PCR-*ig7*	FP- TGAATTGAAGTCTGAGTAAACGG	1795-1817
		RP- TAGATAGGGACCAAACTGTCTCAC	3,065-3,042
3	*In situ*	FP- ATGCTCTAGAACAACAACAAGATGATGATGAT	1372-1393
		RP-TAATGCGGCCGCTGAGTAAAGACCATAGAGTAA	2060-2080
4	*sesn*^{OE}	FP- CGTAGAGCTCAGTATGGGAATGACAAGTAAAGGC	7 to 30
		RP- CTGACTCGAGACCTTCTATTTTGATAATTCATTACTGAG	2076 -2104
5	*sesn* $^{-}$ Frag 1	FP- AGTCCTGCAGTGGTAACAGCTCCTCAGAATG	54-74
		RP- ATGCAAGCTTAATACTGTTGTTCTTTGTTTGG	705-726
6	*sesn* $^{-}$ Frag 2	FP- ATGCTCTAGAACAACAACAAGATGATGATGAT	1795-1817
		RP- TAATGCGGCCGCTAGATAGGGACCAAACTGTCTCAC	3,065-3,042
7	*sesn* KO screening	AACGGTAGTTGCGCCTCTCAA	−828 to -807
8	*sesn* KO screening	GAGATTTTTTGAATTCTAATTAT	3000 to 3023
9	RT-PCR-*ampk* (*snfa*)	FP-ATGAGTTCATATCAACAAAATCCCATTGG	1-29
		RP-CACCATATGATGATGACAATAGTCTACACC	600-630 (421-450 for cDNA)

in dark at room temperature till the satisfactory color was obtained. The reaction was stopped with 1x PBS and the structures were photographed under stereomicroscope (Olympus SMZ32) (Escalante and Loomis, 1995).

2.4. Construction of mutants

Ddsesn overexpressing strain, [(*act15/sesn-eyfp*)/Ax2*; sesn*^{OE}]: *Ddsesn* gene was PCR amplified (Table 1) from the genomic DNA and expressed under *actin15* promoter as a fusion protein with enhanced yellow fluorescence (*eyfp*) reporter gene at the C-terminus and a 6x-His tag at the N-terminus (Saran and Schaap, 2004). It was transformed by electroporation into Ax2 cells and the transformants were selected with antibiotic G418 at 40 µg/ml (maximum) (Gosain et al., 2012).

Ddsesn knockout strain, [*sesn*$^{-}$/Ax2]: The 5′ and 3′ targeting regions were PCR amplified (Table 1) and introduced into the flanking sides (XbaI/HindIII) of the Blasticidin (Bsr) cassette (Fig. S2 A). After restriction digestion with PstI/HindIII, a linearized fragment of 2.95 kb fragment was introduced into Ax2 cells by electroporation and selected at 10 µg/ml of Blasticidin S. Genomic DNA was extracted and targeted gene disruptions were identified by several PCR reaction and further confirmed by sequencing and RT-PCR (Fig. S2B-G).

Expressing the *sesn-eyfp* fusion construct into the *sesn*$^{-}$ cells made the rescue strain.

2.5. Detection of intracellular ROS levels

Dihydroethidium (DHE) dye was used for both flow cytometry and microscopic detection of intracellular ROS levels. Briefly, cells from various strains (Ax2, *sesn*^{OE}, *sesn*$^{-}$, *sesn*^{res}) were harvested, washed and suspended in 1xKK_2 buffer for 2 h at a density of 6×10^6 cells/ml and incubated with 30 µM of DHE under dark for 30 min (Zhang and Soldati, 2013). To measure the ROS levels in vegetative cells, cells were harvested from the exponential phase and washed twice with low fluorescence axenic media (Kim et al., 2007) to remove background green fluorescence signal of the HL5 culture medium and incubated further for 30 min. in the same low fluorescence media followed by repeated washings with 1x KK2 buffer. The fluorescence signal was monitored in FL3 channel using Cell-Quest software (Becton Dickinson, FACS Calibur) and also visualized under the fluorescence microscope (Nikon using Andor iQ 2.7.1 software).

2.6. Autophagy analyses

2.6.1. Autophagic flux

Autophagic flux, in Ax2 and *sesn*$^{-}$ cells, both under control and induced conditions were analyzed using confocal microscopy and proteolytic cleavage (Lohia et al., 2017). In brief, both the cells were transfected with a construct expressing the autophagic marker RFP-GFP-Atg8 as described previously (Lohia et al., 2017). Transformed cells were then induced by starvation stimulus (cells grown in HL5 were washed two times and incubated for 4 h in 1xKK_2 buffer) and treated with the lysomotropic agent NH_4Cl (100 mM for 4 h). The cells were visualized by confocal microscopy and Z-stacks were selected to get the maximum projections covering the whole cell. Autophagic flux was monitored as described earlier (Lohia et al., 2017). For the proteolytic cleavage analysis, an equal amount of protein from both control and induced (NH_4Cl) cells was loaded onto a 10% SDS–PAGE gel. Western blotting was carried out to detect the cleaved GFP and GFP-Tkt-1 fragments using α-GFP antibody (Sigma-Aldrich) (Lohia et al., 2017). We were unable to analyze the same with *sesn*^{OE} cells as we could not distinguish the GFP (in RFP-GFP-Atg8 construct) from and Eyfp (in sesn-Eyfp construct) fluorescence.

2.6.2. Immunoblot

Western blotting was performed to observe the levels of TOR using anti-TOR antibody (Sigma: SAB4501040) and anti-rabbit HRP-conjugated secondary antibody (Genei: 621140380011730) at a dilution of 1:1000 and 1:10,000, respectively (Swer et al., 2016). The expression levels of 4E-BP1 and p4E-BP1 were measured using the antibodies, anti-4E-BP1 and anti-phospho-4E-BP1 at a dilution of 1:8000 each (Swer et al., 2014a, 2016). The secondary anti-goat HRP conjugated antibody was used (Sigma: A5420) at a dilution of 1:10,000. Similarly, the expression levels of AMPK and pAMPK were measured using the antibodies anti-AMPK and anti-phospho-AMPK (Annesley et al., 2011). The RT-PCR of the *ampk* gene (also known as *snfA,* which corresponds to the catalytic α subunit of AMPK) was analyzed using the primer combinations given in Table 1.

Relative amount of protein was calculated by taking the ratios between the integrated density values (idv) of protein of interest and the control protein (used for normalization) and graph was plotted. The idv value was obtained using the alpha imager 3400 software.

2.7. Statistical analysis

In the present study, minimum of 3–5 independent experiments in duplicates or triplicates were performed. The statistical analyses were

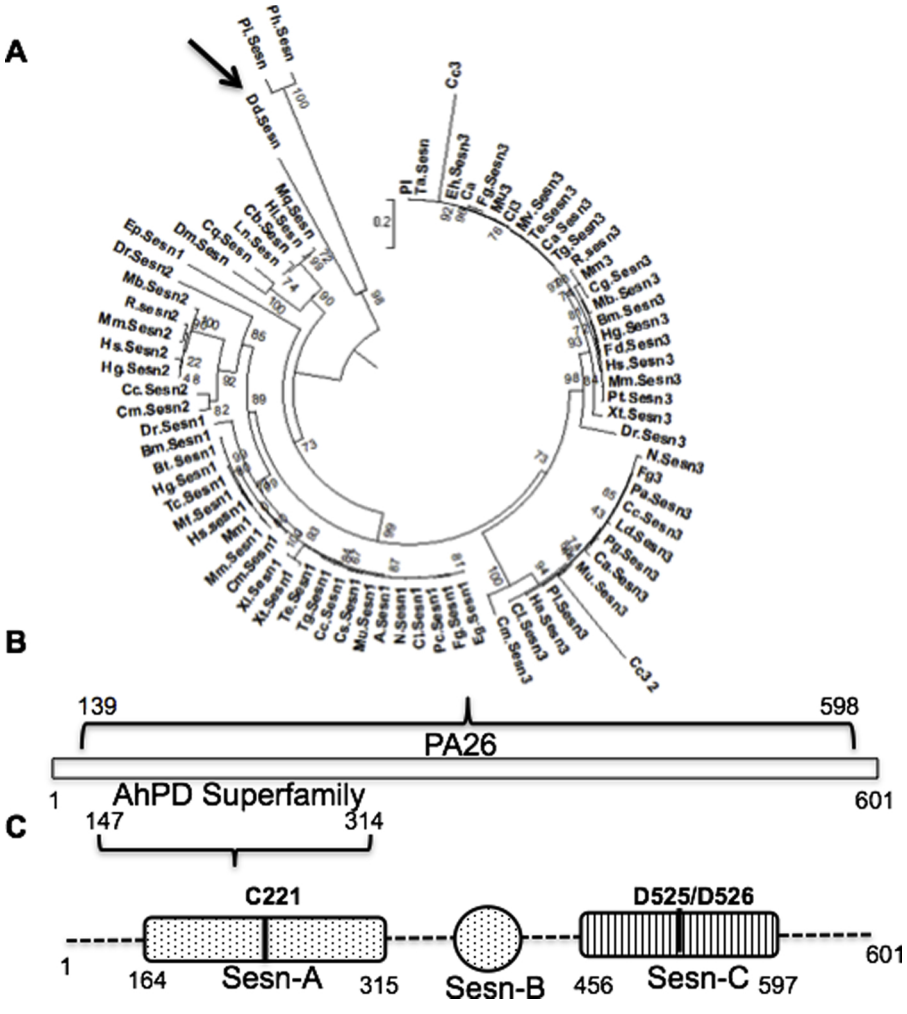

Fig. 1. Single DdSesn-like protein shows two putative functional domains.
(A) Maximum Likelihood (ML) phylogenetic tree of Sesn in Newick format. Sesn protein sequences from Plasmora halstedii (Ph), Phytophthora infestans (Pi), Melipona quadrifasciata, (Mq), Habropoda laboriosa (Hl), Lasius niger (Ln), Culex quinquefasciatus (Cq), *Corvus brachyrhynchos* (Cb), Drosophila melanogaster (Dm), Echinacea pallida (Ep), Danio rerio (Dr), Myotis brandtii (Mb), Rattus norvegicusz (Rn), Macaca mulatta (Mm), Homo sapiens (Hs), Hymenocoleus glaber (Hg), Conuropsis carolinensis (Cc), *Chelonia mydas* (Cm), Bulent mutus (Bm), Bos Taurus (Bt), Tupaia chinensis (Tc), Macaca fascicularis (Mf), *Mus musculus* (Sesn1), Xenopus laevis (Xl), Xenopus tropicalis (Xt), Tauraco erythrolophus (Te), Tinamus guttatus (Tg), Cyathus striatus (Cs), Mesitornis unicolor (Mu), Amazona aestiva (A Sesn1), Netechma notabilis (N Sesn1), Potamogeton cristatus (Pc), *Fulmarus glacialis* (Fg), Egretta garzetta (Eg), *Columba livia* (Cl), Haliaeetus albicilla (Ha), Phaethon lepturus (Pl), *Cuculus canorus* (Ca) (Sesn3), *Cathartes aura* (Ca), Pterocles gutturalis (Pg), Leptosomus discolour (Ld), Calypte anna (Ca), Pseudoseisura gutturalis (Pg), Pygoscelis adeliae (Pa), Fulmaris glacialis (Fg), Nipponi nippon (Nn) (Sesn3), Xenopus tropicalis (Xt), Pan troglodytes (Pt), Fucomys damarensis (Fd), Cricetulus griseus (Cg), Manacus vitellinus (Mv), Eurypyga helias (Eh), *Tyto alba* (Ta) were selected from NCBI data base and subjected to multiple sequence alignment.
(B) The domain analysis as predicted by Pfam program. There are two domains: PA26- whose functions are still unknown and AhPD- that play a role in defense response.
(C) Schematic representations of the domain organization of DdSesn as predicted from multiple sequence alignments performed with the full-length DdSesn protein sequence and the individual known domains of HsSesn2.

performed (mean standard deviation and standard error) and values were plotted in graph using Microsoft Excel-2013 and GraphPad PRISM. The significance value was considered as * $p < 0.05$, ** $p < 0.01$, and *** $p < 0.001$.

3. Results and discussion

3.1. Sestrin-like-protein from D. discoideum shows homology with other Sesn proteins and has both the functional domains

According to dictyBase, (www.dictybase.org) the *D. discoideum* genome encodes one *sestrin-like* gene, (*Dd*sesn; gene id: DDB_G0279427) located on chromosome 3 between coordinates 2032053–2034159. It is a single copy gene having three exons and two introns (2107 bp). It encodes a 601 amino acids protein with a molecular mass of 68.4 kDa. Based on the amino acid sequence, the putative *Dd*Sesn shows 48% similarity to *D. melanogaster*, 30–35% with human Sesn and 22% with *C. elegans* (NCBI database). Phylogenetic analysis showed DdSesn formed a clade with invertebrates and also showed similarity to metazoan Sesn (Fig. 1A)

DdSesn possess two significant domains (Fig. 1B), PA26 (139–598 amino acids), corresponding to the p53 inducible protein whose functions are still not characterized and the AhPD superfamily domain (147–314 amino acids), which represents the α-helical domain found in alkyl-hydroperoxide reductase (AhPD). This is a component of alkyl-hydroperoxide reductase participating in the defense against ROS. The C-terminal α-helical domain of the AhPD protein from *Mycobacterium tuberculosis* shares protein sequence and structural similarity with the N-terminal of Sesn from animals (Budanov et al., 2004).

The crystal structure of human Sesn2 shows two-fold pseudo-symmetry with two globular subdomains, which are structurally similar but functionally distinct from each other. Their findings suggest the molecular mechanism of how Sesn can attenuate degenerative processes like aging and diabetes by acting as a simultaneous inhibitor of ROS accumulation and mTORC1 activation. They found 23 helices and no β-sheets (Kim et al., 2015). Keeping this in mind, we tried to predict the secondary and tertiary structures of DdSesn using Phyre2 server (http://www.sbg.bio.ac.uk.phyre2). We found 26 helices and no β-sheets in DdSesn (Fig. S3). As predicted for human Sesn2, the three domains (Sesn-A to C) were also present in DdSesn (Fig. 1C). Sesn-A domain of HsSesn2 corresponding to 66–239 amino acids showed conservation in 164–315 amino acids region of DdSesn protein sequence; Sesn-B domain of HsSesn2 corresponding to 254–294 amino acids showed less conservation with DdSesn protein sequence and Sesn-C domain of HsSesn2 corresponding to 308–480 amino acids showed conservation with the 456–597 amino acids region of DdSesn protein sequence. The Sesn-A domain of DdSesn showed conserved cysteine residue at 221 position similar to that of the catalytic cysteine residue of HsSesn2 present at position 125, which exhibits antioxidant function while Sesn C domain of DdSesn2 showed the conserved residues at D525, D526 positions similar to that of human Sesn2 of residues D405, D406 that play a key role in the activation of AMPK and suppression of mTORC1.

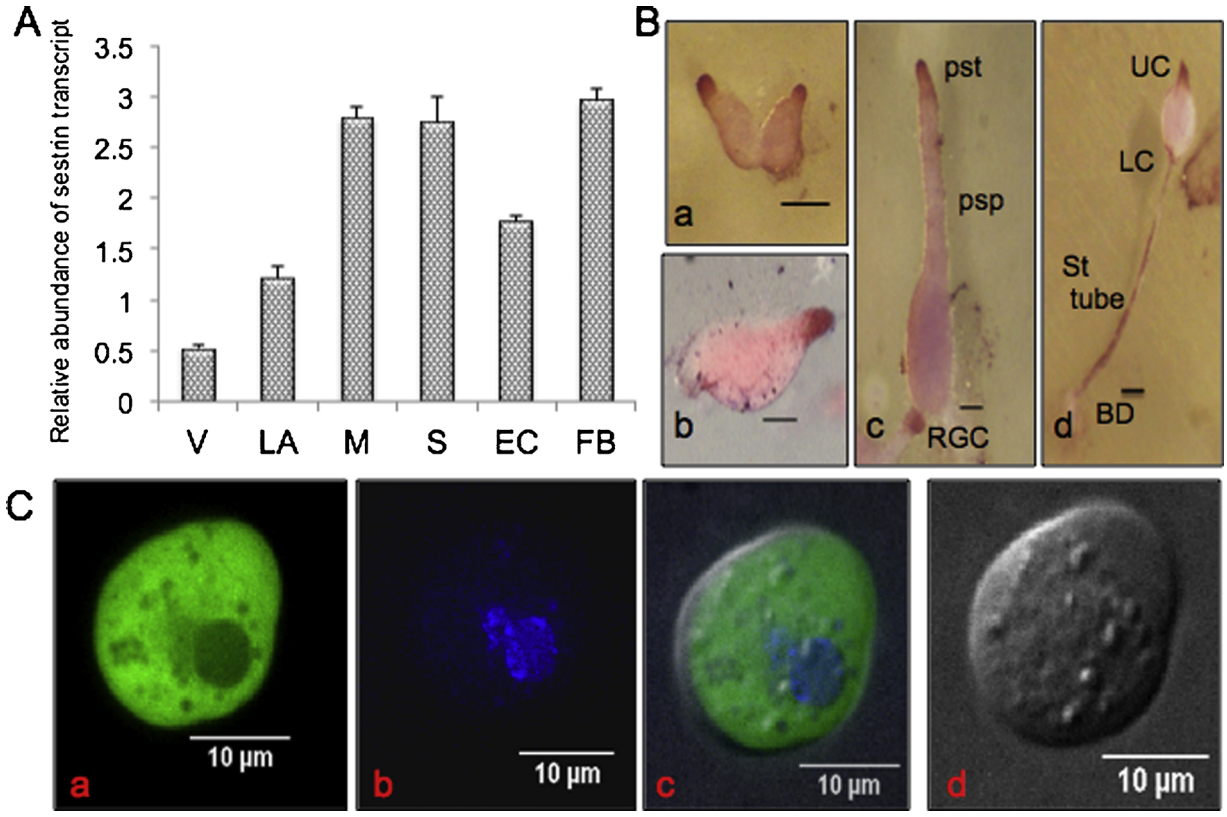

Fig. 2. *Ddsesn* transcript is expressed throughout growth and development and show prestalk localization.
(A) Relative abundance of *Ddsesn* transcript as measured by RT-PCR during development. *rnlA (ig7)* was taken as an internal control. [n = 4; V-Vegetative; LA-Loose Aggregate, M-Mound, S-Slug, EC-Early Culminant and FB-Fruiting Body].
(B) Spatial mRNA expression as studied by *in situ* hybridization in multicellular structures developed. The transcript shows prestalk localization. [a-first finger; b-standing slug; c- migrating slug, d: fruiting body; pst-prestalk; psp-prespore; st tube-stalk tube; BD-basal disc; UC-upper cup; LC-lower cup; RGC-rear guard cells; scale bar: 100 µm; n = 3].
(C) Subcellular localization of Sesn-eYFP [a-Green due to Sesn-eYFP fusion protein; b-Blue due to DAPI in nucleus; c-merged image; d-DIC image; scale bar: 10 µm].

3.2. DdSesn mRNA is expressed in prestalk/stalk cells

We analyzed the spatiotemporal mRNA expression patterns both by reverse transcriptase PCR (RT-PCR) and *in situ* hybridization. The *sesn* transcript was present throughout growth and development, showing minimum levels in the vegetative cells and increased levels during multicellular development except for a small dip during early culmination (Fig. 2A). The whole mount *in situ* hybridization analyses showed the *sesn* transcript to be present at all stages of development and mainly localized in the prestalk/stalk regions of multicellular structures developed (Fig. 2B). The expression was nearly absent in the rear-guard cells (Fig. 2Bc) of the migrating slug. The expression was present in the stalk, lower and upper cups of the culminant. There was low expression in the basal disc (Fig. 2Bd). On the other hand, use of sense probe gave no specific results (Fig. S1B).

In conclusion, *sesn* transcript showed prestalk localization and was expressed throughout growth and development.

3.3. Making of sesn mutants

To investigate the functions of Sesn, we created both overexpressing [(*act15/sesn-eyfp*)/Ax2; $sesn^{OE}$] and deletion ($sesn^{-}$/Ax2) mutants (Fig. S2E, F, G). The rescue [(*sesn-eyfp*)/$sesn^{-}$; $sesn^{res}$] strain performed more or less like the wild type strain. The fusion protein showed cytosolic localization (Fig. 2C). We found approximately four-fold increase in the *sesn* transcript levels over the wild type in the $sesn^{OE}$ cells (Fig. S2F).

3.4. Sesn suppress cell growth and deletion of sesn gene results in multi-tipped structures

To measure the rate of cell growth in liquid culture, Ax2, $sesn^{OE}$, $sesn^{-}$ and $sesn^{res}$ log phase cells were identically diluted into fresh media at equal cell density and monitored over several days (Fig. 3A). Ax2 cells reached stationary phase at a cell density of 1.40×10^7 cells/ml by t_{60} and did not display a decline phase till 96 h. $sesn^{OE}$ cells reached a cell density of 1.08×10^7 cells/ml by t_{72} and showed a decline phase hence after. Also, a longer lag phase till t_{24} was observed. $sesn^{-}$ cells reached a cell density of a 1.48×10^7 cells/ml by t_{60} and did not show a decline phase till 96 h. The $sesn^{res}$ strain also showed near similar growth as the Ax2 cells reaching maximum cell density of 1.4×10^7 cells/ml by t_{60}. The doubling time for $sesn^{OE}$, $sesn^{-}$, Ax2 and $sesn^{res}$ cells were 20.4 $\pm$ 1.34 h, 10.98 $\pm$ 0.74 h, 11.8 $\pm$ 1.34 h and 10.5 $\pm$ 1.21 h, respectively. Taken together, the data suggest that Sesn regulates cell growth in *Dictyostelium*.

Since the $sesn^{OE}$ cells showed slower cell growth we checked for their size and compared them to Ax2 cells (Fig. 3B). The $sesn^{OE}$ cells were smallest in size. $sesn^{-}$ cells was larger than the $sesn^{OE}$ cells but smaller than the wild type cells. The $sesn^{res}$ showed similar cell size as that of $sesn^{-}$ cells.

To examine the role of Sesn in multicellular development we plated cells from various strains at equal densities on non-nutrient agar plates and allowed them to develop after synchronization (Fig. 3C, Fig. S4). Ax2 cells completed their development by forming aggregates by 6 h, mounds by 8 h, slugs by 16 h and fruiting bodies by 24 h. $sesn^{OE}$ and $sesn^{-}$ cells exhibit negligible differences with respect to time for

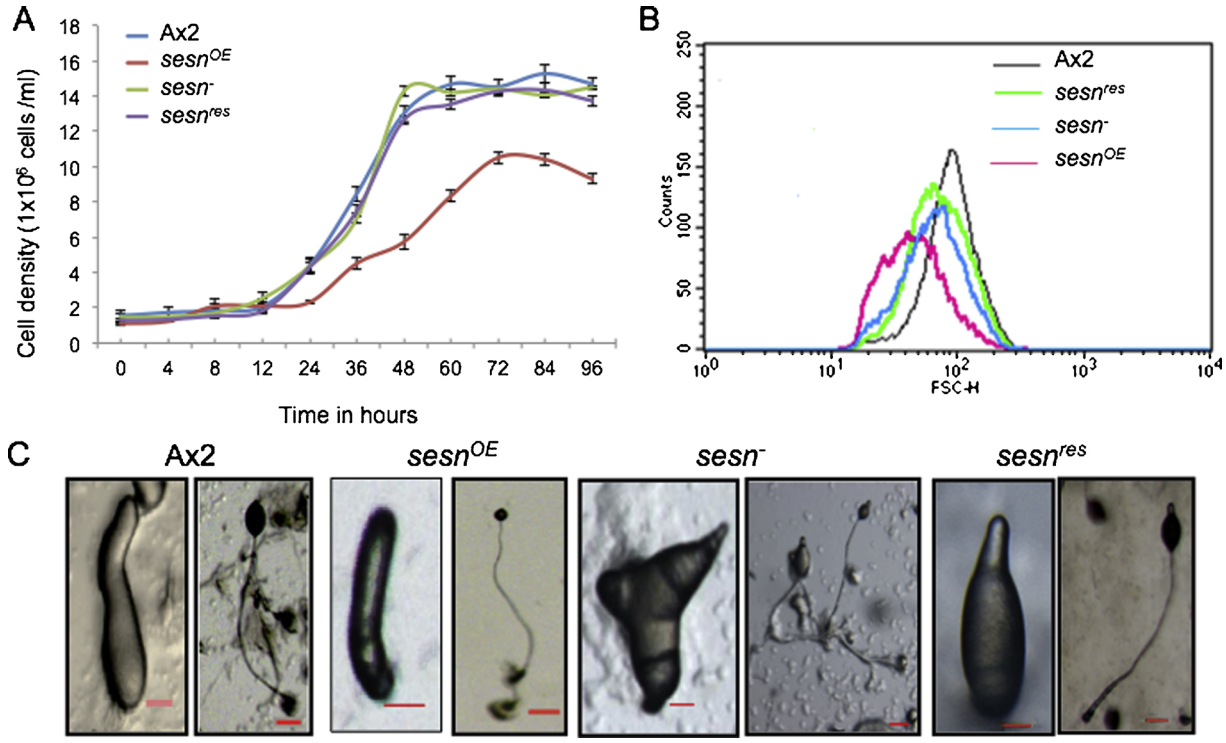

Fig. 3. Analyses of growth and development of mutants.
(A) Growth profile of Ax2, *sesn*^{OE}, *sesn*$^{-}$ and *sesn*^{res} cells. Cells were grown in HL5 medium and at regular time intervals the cells were counted in a haemocytometer. [n = 4].
(B) Forward scatter as a measure of cell size of Ax2, *sesn*^{OE}, *sesn*$^{-}$ and *sesn*^{res} cells. The *sesn*^{OE} cells were smallest in size.
(C) Equal number of mid-log phase culture cells of Ax2, *sesn*^{OE}, *sesn*$^{-}$ and *sesn*^{res} were plated and synchronized for development. Here we show single structures of slugs and fruiting body formed by each strain. A minimum of 5–7 such frames was considered. The *sesn*$^{-}$ cells developed attached to the base. [Scale bar: 100 µm; n = 4].

development as compared to Ax2 cells. *sesn*^{OE} cells developed fewer aggregates of smaller sizes as compared to Ax2 cells. The aggregates developed into fruiting bodies with long slender stalks and small sori (Fig. 3C). The *sesn*$^{-}$ cells formed large-sized aggregates that developed into slugs attached at their bases and appeared multi-tipped. The fruiting bodies developed from such clusters also were attached at the base. Few cluster of slugs failed to migrate and break away from the clusters (Fig. 3C). Fig. S4 A shows development at lower magnification to assess the phenotype.

3.5. DdSesn protect cells from stress by lowering the ROS levels

Here we show that starvation increased ROS levels (Fig. S5C) and was earlier reported by Swer et al. (2014b) that increased ROS levels could induce autophagy in *D. discoideum*. We thus wanted to understand if DdSesn could play a protective role by lowering the ROS levels upon starvation. Our investigation showed a time-dependent increase in the levels of *sesn* transcript upon starvation of Ax2 cells (Fig. 4A and Fig. S5 A, B). To substantiate our findings, we monitored the levels of ROS both by microscopy and FACS using DHE as a marker for ROS measurements in 2 h starved different *sesn* mutants and compared them to Ax2 cells. The fluorescence level was highest in the *sesn*$^{-}$ cells (Fig. 4D), followed by the Ax2 cells and *sesn*^{res} (Fig. 4B, 4E) and the least in the *sesn*^{OE} cells (Fig. 4C, Fig. S5D). The fluorescence intensity is directly related to the levels of ROS in the cells showing highest ROS levels in the *sesn*$^{-}$ cells. We strengthened our results by FACS analysis, which showed, 59.38 ± 4.94% and 59.76 ± 2.2% cells to be ROS positive in Ax2 and *sesn*^{res} strains (Fig. 4J, 4 M). This decreased to 23.95 ± 3.4% in the *sesn*^{OE} cells (Fig. 4K) and increased to 87.38 ± 2.5% in the *sesn*$^{-}$ cells (Fig. 4L). To get a better understanding of the ROS levels in growing cells, we analyzed the same under low-flo (low fluorescence) medium (Fig. 4F-I). The results show a decrease in ROS levels in the Ax2 (34.81± 2.43%), *sesn*$^{-}$ (77.58± 1.2%) and *sesn*^{res} (47.56 ± 2.88%) cells and a small increase in *sesn*^{OE} (28.38 ± 4.4%) cells when compared to 2 h starved cells. Our results suggest an increase in *sesn* expression in case of *sesn*^{OE} cells that could possibly lower the ROS levels generated during control and stress conditions. On the other hand, deletion of *sesn* (*sesn*$^{-}$) increased the ROS positive cells under both the control and starved conditions but the increase was more pronounced in the starved cells (that is 77.58–87.38%; Fig. 4H, L).

Taken together, these results showed that Sesn is not only important during starvation but also plays a role in regulating ROS levels in vegetative cells.

3.6. Up-regulation of DdSesn cause autophagy induction

The signalling pathway that may get affected by the redox activity of Sesn is the target of rapamycin (TOR) kinase (Budanov and Karin, 2008), which is a critical regulator of cell growth, proliferation, translation, metabolism and autophagy. We observed decreased TOR levels in *sesn*^{OE} cells and no significant change in *sesn*$^{-}$ cells over the wild type (Fig. 5A and Fig. S7 shows the specificity of TOR antibody. Our results showed Sesn-dependent reduction of TORC1 signalling. We also analyzed the effect of DdSesn on TOR kinase activity by monitoring the phosphorylated and non-phosphorylated levels of 4E-BP1 (Fig. 5B and Fig S6B). The decrease in phosphorylation levels of 4E-BP in *sesn*^{OE} cells could be due to the reduction of endogenous TOR levels. Thus, our studies indicate, overexpression of DdSesn may decrease the TOR levels, which in turn decrease the phosphorylated 4E-BP1 levels. It was reported that Sesn2 facilitates the free and non-phosphorylated 4E-BP1 to interact with the eIFs resulting in the hampering of translated proteins that are involved in cell growth (Wullschleger et al., 2006). This

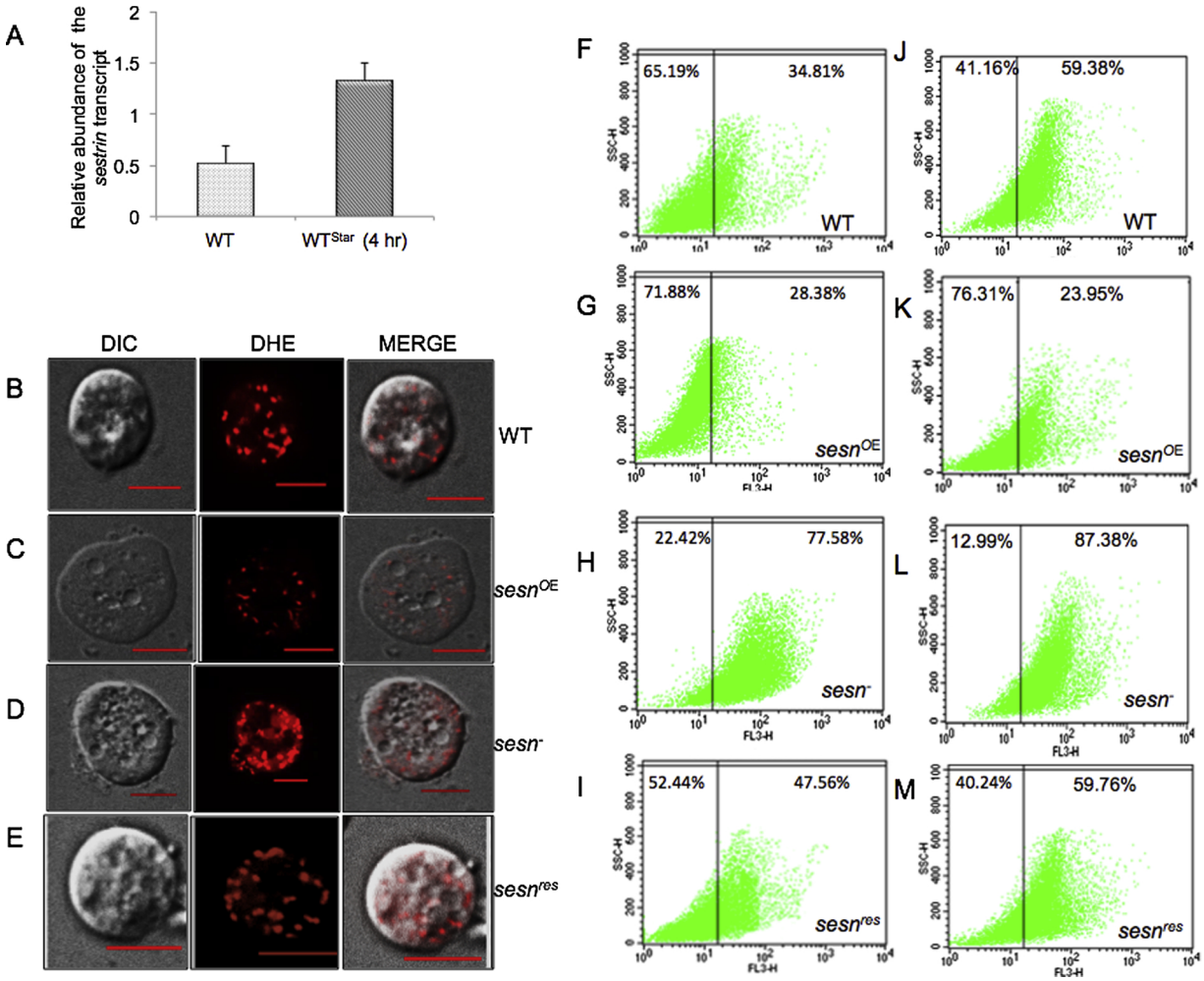

Fig. 4. ROS levels in different *sesn* mutants.

Relative transcript levels of *Ddsesn* as measured by RT-PCR in both growing and starved vegetative cells. Cells were starved for 0–4 h. *ig7* was used as an internal control. [n = 4].

Representative confocal fluorescence images of freshly starved cells stained with DHE. (B) Ax2, (C) $sesn^{OE}$ and (D) $sesn^{-}$ (E) $sesn^{res}$. ·In all the three panels the first image corresponds to DIC, second corresponds to DHE fluorescence and the third is a merged image. [Scale bar: 10 µm; n = 3].

Flow cytometry analysis in low-flo medium (as control) for Ax2 (F), $sesn^{OE}$ (G) and $sesn^{-}$ (H) $sesn^{res}$ (I) cells and in 2 h starved Ax2 (J), $sesn^{OE}$ (K) and $sesn^{-}$ (L) $sesn^{res}$ (M) cells using fluorescent dye Dihydroethidium (DHE).

result reflects our cell growth studies also, where we found slow growth by $sesn^{OE}$ cells as compared to the *sesn*- and Ax2 cells (Fig. 3A). Further, we also observed a decrease in cell size of $sesn^{OE}$ cells while *sesn*- cells showed a small decrease as compared to the Ax2 cells (Fig. 3B). A similar Sesn-dependent suppression of TORC1 signalling with a decrease in cell size was also observed in *Drosophila*, which strengthens the fact that Sesn-dependent regulation of TORC1 signalling is conserved throughout the metazoans. It was seen that overexpression of Sesn resulted in cell size reduction that was mediated by TORC1 inhibition in adult eyes and larval-wing discs of *Drosophila* (Lee et al., 2010). Also, deficiency of *sesn* in both *Drosophila* and mice (Sesn2/3) did not lead to an increase in body size or cell/tissue growth (Lee et al., 2013). Since we observed reduced TOR activity, as reflected by decreased phosphorylated 4E-BP1 (downstream target of TOR) levels in $sesn^{OE}$ cells; we further wanted to investigate the role of DdSesn in autophagy.

We thus asked, if DdSesn up-regulation contributed towards the maintenance of autophagy activity? To answer this, we monitored autophagic flux in both the $sesn^{-}$ and the control Ax2 cells as it is important to analyze not only the autophagosome formation but also whether degradation of the cargos has taken place. Autophagic flux was monitored by puncta count in the tandemly tagged RFP-GFP-Atg8, an autophagosome marker protein (RFP-GFP-Atg8) (Lohia et al., 2017). When the green-red merged images of cells are analyzed, yellow puncta is seen which represent early autophagosomes, while red-only puncta (red that lack green) indicate autolysosomes. Thus, when the autophagic flux is increased both yellow and red puncta increase, however, when there is a blockage in lysosomal fusion or acidification, yellow puncta will accumulate. Treatment with lysosomotropic agent like NH_4Cl partially elevates lysosomal pH and reveals autolysosomes.

We observed an increase in red puncta in Ax2 cells upon starvation (Fig. 6A, left panel; lower magnification Fig. S8A, left panel). Upon treatment with NH_4Cl along with starvation, we observed an increase in yellow puncta but no significant increase in red puncta like in other cases. When a similar experiment was performed with the $sesn^{-}$ cells we found no increase in either red or yellow puncta indicating that deletion significantly blocked the up-regulation of autophagy (Fig. 6A, right panel; lower magnification Fig. S8A, right panel). Also, the levels of yellow and red puncta in the $sesn^{-}$ cells was far less than that

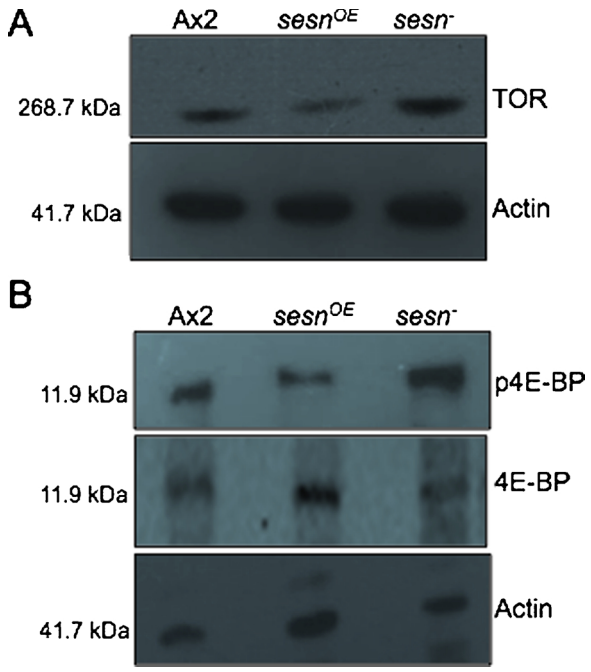

Fig. 5. DdSesn negatively regulates TOR protein.
One representative western blot showing TOR protein expression levels in wild type (Ax2), *sesn*^{OE} and *sesn*$^{-}$ cells using anti-TOR antibody. The level in *sesn*^{OE} cells was reduced while increased in *sesn-* cells as compared to the Ax2 cells. The kinase activity of TOR protein was monitored by observing the levels of phosphorylated (upper panel) and non-phosphorylated (middle panel) levels of its downstream target, eukaryotic translation initiation factor 4E-binding protein, in Ax2, *sesn*^{OE} and *sesn*$^{-}$ cells. Actin (lower panel) was taken as a loading control.

observed with Ax2 cells indicating DdSesn was essential in maintaining the autophagy levels.

Autophagic flux was also measured based on the presence of proteolytic fragments derived from autophagic degradation of expressed fusion protein (Lohia et al., 2017). When GFP is fused to Tkt-1, it is taken and delivered to lysosomes by autophagy, GFP fragments accumulate while the rest of the fusion protein is degraded. GFP cleavage fragments can therefore be quantified by western blot analysis with anti-GFP antibodies. *D. discoideum* has efficient proteolytic machinery and thus free GFP is barely detectable due to rapid degradation. Therefore, treatment with NH_4Cl is required to inhibit proteolysis for the cleaved GFP fragments to accumulate. Band intensities for GFP-Tkt- and free-GFP give a measure of autophagic flux. Cleaved free GFP was visible in NH_4Cl treated Ax2 cells as compared to untreated cells confirming autophagic flux. However, decreased levels of cleaved GFP fragments were observed in both the NH_4Cl treated and untreated *sesn*$^{-}$ cells (Fig. 6C) suggesting that the process of autophagy decreased in the *sesn*$^{-}$ cells. This could be the possible reason for the observed multi-tipped phenotype of *sesn*$^{-}$ cells.

3.7. DdSesn up-regulates phosphorylation of AMPK

It was earlier reported that Sesn2 activated AMPK, which is proposed to be the mediator of longevity and calorie restriction in many systems studied (Hou et al., 2015). AMPK is a heterotrimeric enzyme composed of a catalytic α-subunit and regulatory β and γ subunits. Increase in the intracellular AMP levels, allow it to bind to the γ-subunit and allosterically induces conformational change to allow the phosphorylation on Thr^{188}, which is essential for the kinase activity of AMPK (Sanz et al., 2013). Overexpression of DdSesn resulted in increased phosphorylation of AMPK (Thr^{188}) but not of the total AMPK levels (Fig. 7A, Fig S9). Thus, we conclude that overexpression of DdSesn is associated with increased phosphorylation of AMPK.

Further, we monitored the mRNA levels of *ampk* in Ax2, *sesn*^{OE} and *sesn*– cells in the presence and absence of rapamycin (50 nM for 48 h). We observed increased levels of *ampk* transcript in *sesn*^{OE} and decreased levels in *sesn*– cells when compared to Ax2 cells. The low *ampk* transcript levels observed in rapamycin treated cells could be attributed to the inhibition of TOR. We speculate that rapamycin treatment could prevent the chronic activation of TOR, which prevents the feedback activation of *sesn* and further *ampk* levels (Fig. 7B). This feedback activation of *sesn* was also seen in Drosophila and other mammals (Lee et al., 2010).

In summary, our present study demonstrates DdSesn protects the cells from accumulating ROS upon starvation and is involved in autophagy. We propose overexpression of DdSesn increases the pAMPK and reduces the TOR levels besides having a role in autophagy.

4. Conclusions

Presently we show that starvation induced DdSesn, lowers the ROS levels generated during stress and probably protects them from tremendous toxicity. This decrease in ROS levels could be attributed to its antioxidant activity. Deletion of DdSesn caused accumulation of ROS, which was also observed in other studies where it caused oxidative cell damage, chromosomal instability and cell death (Budanov et al., 2004; Nogueira et al., 2008; Lee et al., 2010). In our studies we observed that deletion of *sesn* led to the accumulation of ROS but not to cell death as the *sesn*$^{-}$ cells showed normal growth and development except for few minor discrepancies. This could be attributed to the presence of possible effective antioxidant pathways or proteins that may help overcome the deleterious effects of ROS to ensure cell viability. We showed deletion of DdSesn resulted in ROS accumulation, while overexpression reduced the ROS levels, suggesting DdSesn may possess putative antioxidant activity, which help in reducing the intracellular ROS levels that were generated during starvation (stress) conditions. The detailed mechanism regarding antioxidant property of DdSesn is yet to be analyzed. In the current study, we also observed insignificant changes in the expression level of *sesn* transcript when wild type cells were treated with H_2O_2 (0.5 mM for 60 min, Garcia et al., 2000) and with antioxidant, NAC (0.5 mM for 60 min Swer et al., 2014a) suggesting that ROS generated had no effect on *sesn* transcript level at the vegetative state. However, future studies are still required to understand the effects during development (Fig. S10).

Further, our results also suggest that DdSesn is involved in the reduction of TOR and phosphorylated 4E-BP levels. We chose vegetative cells for the analysis (cells directly from HL5 medium) as it is reported that the TOR activity gets highly activated in nutrient-rich conditions while under nutrient-depletion state the activity is decreased (Rosel et al., 2011). Besides, the expression of TOR protein is nearly absent till up to 6 h of starvation during development (Swer et al., 2016). Therefore, as TOR levels are abundant in vegetative cells and lower in the starved cells, it is easy to study and compare them. In case of *Drosophila* and few other systems, Budanov and group (Budanov and Karin, 2008; Budanov et al., 2010) have shown that Sestrins suppress the TOR levels and its activity but in *Dictyostelium* we observed that there was reduction of TOR levels and its activity. This could be attributed to the fact that *TOR* is an essential gene whose product may be required for cell survival (Swer et al., 2016). Since these cells still have the ability to grow and develop we expect TOR activity to be only reduced and not completely suppressed.

The expression pattern of *sesn* transcript observed during

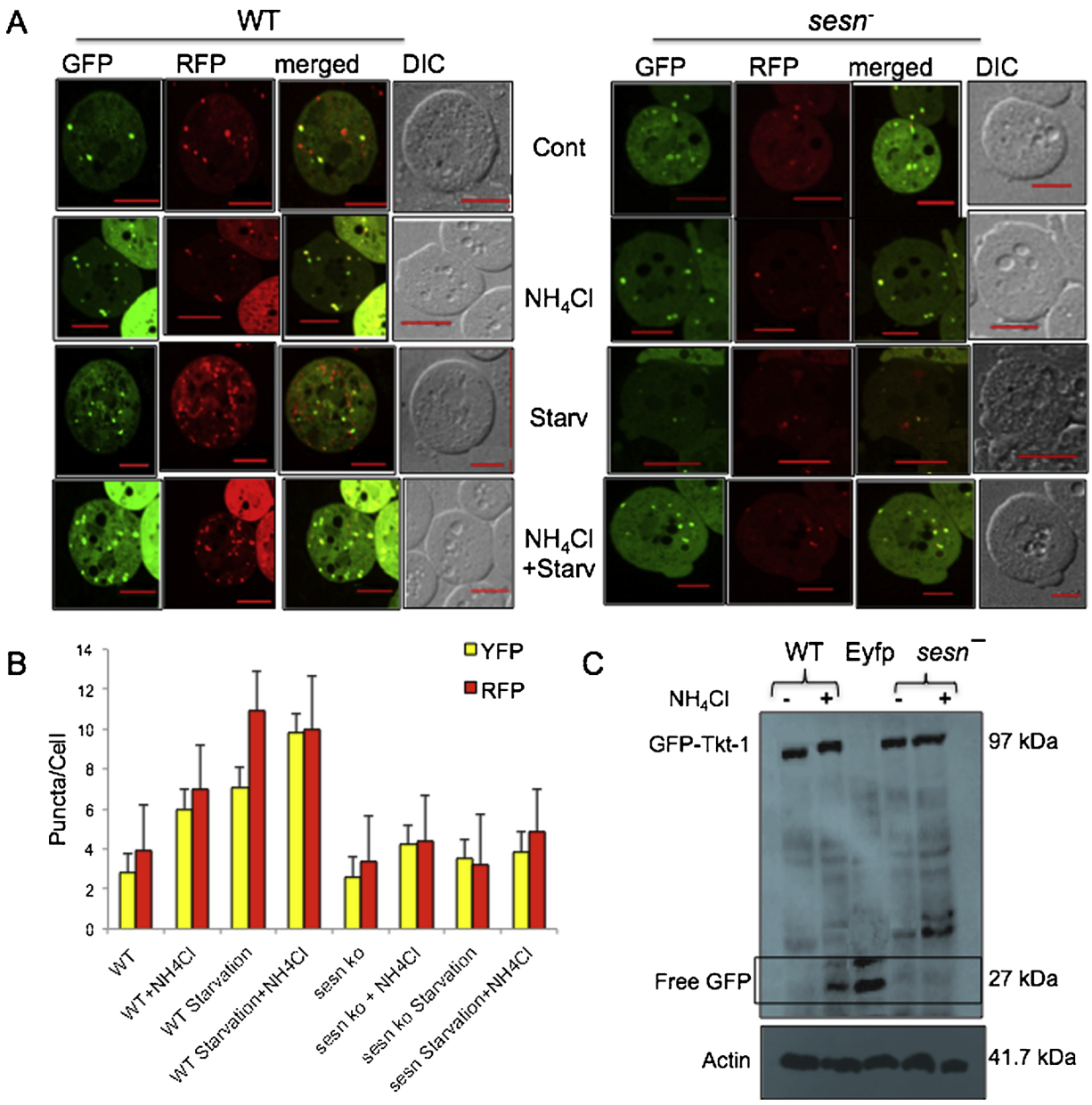

Fig. 6. Deletion of DdSesn showed reduced autophagic flux.
(A)Confocal images of Ax2 (left panel) and *sesn*$^-$ (right panel) cells transformed with tandemly tagged RFP-GFP-Atg8 construct under control, NH_4Cl treated, starvation-induced and both starvation and NH_4Cl treated conditions.
(B)Atg8 puncta/cell were counted in Ax2 and *sesn*$^-$ cells under various conditions using NIS-elements software. A total of 100-cells/individual experiment were analyzed for each condition and statistical significance was calculated using two-way ANOVA [scale bar: 10 μm; n = 5]
(C)One representative western blot showing proteolytic cleavage as a measure of autophagic flux. Both Ax2 and *sesn*$^-$ cells were transfected with the marker GFP-Tkt-1 and grown with 0 or 100 mM NH_4Cl. Equal amount of protein was subjected to SDS–PAGE, transferred onto the membrane and incubated with α-GFP antibody to detect GFP-Tkt-1 and the cleaved GFP proteins. [Lane 3 shows positive control with eYFP].

development is antagonistic to that of *TOR* transcript (Swer et al., 2016). The less availability of *sesn* transcript at the initial stages of development favours the abundant expression of *TOR* transcript while gradual increase in expression of *sesn* transcript during later stages of development (that is after aggregation stage) decreases the *TOR* transcript levels, suggesting that *sesn* transcript may negatively regulate the *TOR* transcript levels during development. However, the absence of TOR protein at early stages of development (Swer et al., 2016) could be due to the quick response of Sestrin protein upon nutritional stress that may inhibit TOR protein and induce autophagic cell death during development. This is just a speculation as we failed to check the expression of Sesn protein during development because unavailability of specific Sestrin antibody.

Thus, this study sheds light on a novel function of starvation-induced DdSesn, which induces autophagic cell death and inhibits cell growth that provide the basis for the identification of new pharmacological targets for drug discovery in most of the cancers. However, a lot more research is called for to understand the regulatory mechanisms

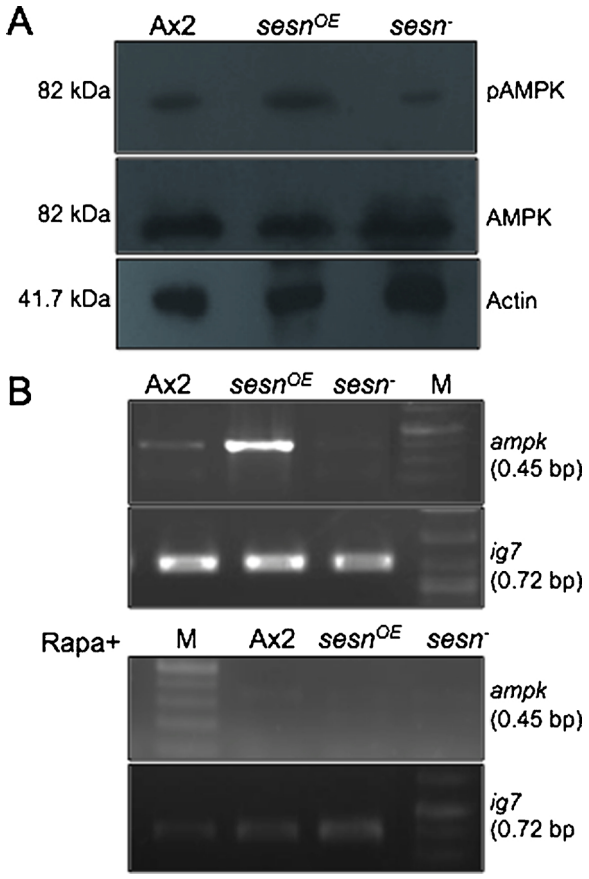

Fig. 7. DdSesn activates AMPK expression.
(A)Western blot showing high pAMPK protein level in the *sesn*^{OE} cells as compared to Ax2 and *sesn*$^{-}$ cells. Here one representative western blot for each probe is shown.
(B)The transcript level of *ampk* in panel 1 was measured in Ax2, *sesn*^{OE}, *sesn*$^{-}$ cells while the panel 2 shows *ig7* in the same cells as panel 1. Panel 3, shows the *ampk* transcript levels after rapamycin treatment in Ax2, *sesn*^{OE}, *sesn*$^{-}$ cells while panel 4 shows *ig7* levels in the same cells.

required for the interaction of DdSesn with the AMPK/TOR signalling cascade.

Conflict of interest

There is no conflict of interest.

Acknowledgements

SS thanks partial grants from DST-PURSE, UPE-II and FIST-II. SR thanks UGC for research fellowship. We thank the Central Instrumentation Facility, SLS for both microscopy and FACS facilities.

Appendix A. Supplementary data

Supplementary material related to this article can be found, in the online version, at doi:https://doi.org/10.1016/j.micres.2018.12.006.

References

Annesley, S.J., Bago, R., Mehta, A., Fisher, P.R., 2011. A genetic interaction between NDPK and AMPK in *Dictyostelium discoideum* that affects motility, growth and development. Naunyn Schmiedebergs Arch. Pharmacol. 384 (4-5), 341–349.

Bae, S.H., Sung, S.H., Oh, S.Y., Lim, J.M., Lee, S.K., et al., 2013. Sestrins activate Nrf2 by promoting p62-dependent autophagic degradation of Keap1 and prevent oxidative liver damage. Cell Metab. 17, 73–84.

Budanov, A.V., Karin, M., 2008. P53 target genes sestrin1 and sestrin2 connect genotoxic stress and mTOR signaling. Cell 134, 451–460.

Budanov, A.V., Shoshani, T., Faerman, A., Zelin, E., Kamer, I., et al., 2002. Identification of a novel stress-responsive gene Hi95 involved in regulation of cell viability. Oncogene 21, 6017–6031.

Budanov, A.V., Sablina, A.A., Feinstein, E., Koonin, E.V., Chumakov, P.M., 2004. Regeneration of peroxiredoxins by p53-regulated Sestrins, homologs of bacterial AhpD. Science 304, 596–600.

Budanov, A.V., Lee, J.H., Karin, M., 2010. Stressin' Sestrins take an aging fight. EMBO Mol. Med. 2, 388–400.

Chen, C.C., Jeon, S.M., Bhaskar, P.T., Nogueira, V., Sundararajan, D., et al., 2010. FoxOs inhibit mTORC1 and activate Akt by inducing the expression of Sestrin3 and Rictor. Dev. Cell 18 (4), 592–604.

Dereeper, V., Guignon, G., Blanc, S., Audic, S., Buffet, S., et al., 2008. Phylogeny fr: robust phylogenetic analysis for the non-specialist. Nucleic Acids Res. 36, W465–W469.

Edgar, R.C., 2004. MUSCLE: multiple sequence alignment with high accuracy and high throughput. Nucleic Acids Res. 32, 1792–1797.

Escalante, R., Loomis, W.F., 1995. Whole mount in situ hybridization of cell type specific mRNAs in Dictyostelium discoideum. Develop. Biol. 171, 262–266.

Garcia, M.X.U., Foote, C., Van Es, S., Devreotes, P.N., Alexander, S., Alexander, H., 2000. Differential developmental expression and cell-type specificity of *Dictyostelium* catalases and their response to oxidative stress and UV-light. Biochim. Biophys. Acta (Gene Struct. Express.) 1492 (2-3), 295–310.

Gosain, A., Lohia, R., Shrivastava, A., Saran, S., 2012. Identification and characterization of peptide: N-glycanase from Dictyostelium discoideum. BMC Biochem. 13 (1), 9.

Guindon, S., Gascuel, O., 2003. A simple, fast, and accurate algorithm to estimate large phylogenies by maximum likelihood. Sys. Biol. 52 (5), 696–704.

Guindon, S., Lethiec, F., Duroux, P., Gascuel, O., 2005. PHYML Online—a web server for fast maximum likelihood-based phylogenetic inference. Nucleic Acids Res. 33, W557–W559.

Hou, Y.S., Guan, J.J., Xu, H.D., Wu, F., Sheng, R., Qin, Z.H., 2015. Sestrin2 protects dopaminergic cells against rotenone toxicity through AMPK-dependent autophagy activation. Mol. Cell. Biol. 35, 2740–2751.

Kim, H.L., Choi, Y.K., Kim, D.H., Park, S.O., Han, J., Park, Y.S., 2007. Tetrahydropteridine deficiency impairs mitochondrial function in *Dictyostelium discoideum* Ax2. FEBS Lett. 581 (28), 5430–5434.

Kim, H., An, S., Ro, S.H., Teixeira, F., Park, G.J., et al., 2015. Janus-faced Sestrin2 controls ROS and mTOR signalling through two separate functional domains. Nat. Comm. 6, 10025.

King, J.S., 2012. Autophagy across the eukaryotes: is *S. Cerevisiae* the odd one out? Autophagy 8, 1159–1162.

Klionsky, D.J., Abdelmohsen, K., Abe, A., Abedin, M.J., Abeliovich, H., Acevedo Arozena, A., et al., 2016. Guidelines for the use and interpretation of assays for monitoring autophagy. Autophagy 12 (1), 1–222.

Lee, J.H., Budanov, A.V., Park, E.J., Birse, R., Kim, T.E., et al., 2010. Sestrin as a feedback inhibitor of TOR that prevents age-related pathologies. Science 327, 1223–1228.

Lee, J.H., Budanov, A.V., Talukdar, S., Park, E.J., Park, H.L., et al., 2012. Maintenance of metabolic homeostasis by Sestrin2 and Sestrin3. Cell Metabol. 16, 311–321.

Lee, J.H., Budanov, A.V., Karin, M., 2013. Sestrins orchestrate cellular metabolism to attenuate aging. Cell Metabol. 18, 792–801.

Lohia, R., Jain, P., Jain, M., Burma, P.K., Shrivastava, A., Saran, S., 2017. *Dictyostelium discoideum* Sir2D protein, an ortholog of human 1 SIRT1, modulates cell type specific gene expression and is involved in autophagy. Phys. Med. 61 (1-2), 95–104.

Nogueira, V., Park, Y., Chen, C.C., Xu, P.Z., Chen, M.L., et al., 2008. Akt determines replicative senescence and oxidative or oncogenic premature senescence and sensitizes cells to oxidative apoptosis. Cancer Cell 14, 458–470.

Peeters, H., Debeer, P., Bairoch, A., Wilquet, V., Huysmans, C., et al., 2003. PA26 is a candidate gene for heterotaxia in humans: identification of a novel PA26-related gene family in human and mouse. Hum. Genet. 112, 573–580.

Rosel, D., Khurana, T., Majithia, A., Huang, X., Bhandari, R., Kimmel, A.R., 2011. TOR complex 2 (TORC2) in *Dictyostelium* suppresses phagocytic nutrient capture independently of TORC1-mediated nutrient sensing. J. Cell. Sci. 125, 1–12.

Sanz, P., Rubio, T., Garcia, M.A., 2013. AMPK beta subunits: more than just a scaffold in the formation of AMPK complex. FEBS J. 280, 3723–3733.

Saran, S., Schaap, P., 2004. Adenylyl cyclase G is activated by an intramolecular osmosensor. Mol. Biol. Cell 15 (3), 1479–1486.

Schaap, P., 2011. Evolution of developmental cyclic adenosine monophosphate signalling in the Dictyostelia from an amoebozoan stress response. Dev. Growth Diff. 53 (4), 452–462.

Showkat, M., Beigh, M.A., Andrabi, K.I., 2014. mTOR signaling in protein translation regulation: implications in cancer genesis and therapeutic interventions. Mol. Biol. Inter. 2014, 686984.

Swer, P.B., Bhadoriya, P., Saran, S., 2014a. Analysis of Rheb in the cellular slime mold *Dictyostelium discoideum*: cellular localization spatial expression and overexpression. J. Biosci. 39, 75–84.

Swer, P.B., Lohia, R., Saran, S., 2014b. Analysis of rapamycin induced autophagy in Dictyostelium discoideum. Ind. J. Exp. Biol. 52, 295–304.

Swer, P.B., Mishra, H., Lohia, R., Saran, S., 2016. Overexpression of TOR (target of rapamycin) inhibits cell proliferation in Dictyostelium discoideum. J. Basic Micro. 56

(5), 510–519.
Tamura, K., Stecher, G., Peterson, D., Filipski, A., Kumar, S., 2013. MEGA6: molecular evolutionary genetics analysis version 60. Mol. Biol. Evol. 30 (12), 2725–2729.
Velasco-Miguel, S., Buckbinder, L., Jean, P., Gelbert, L., Talbott, L.R., et al., 1999. PA26, a novel target of the p53 tumor suppressor and member of the GADD family of DNA damage and growth arrest inducible genes. Oncogene 18, 127–137.
Whittingham, W.F., Raper, K.B., 1960. Non-viability of stalk cells in Dictyostelium. Proc. Nat. Acad. Sci. 46 (5), 642–649.
Wullschleger, S., Loewith, R., Hall, M.N., 2006. TOR signalling in growth and metabolism. Cell 124, 471–484.
Zhang, X., Soldati, T., 2013. Detecting, visualizing and quantitating the generation of reactive oxygen species in an Amoeba model system. J. Vis. Exp. 81, 50717.